

Quantum Signatures of the Optomechanical Instability

Jiang Qian,¹ A. A. Clerk,² K. Hammerer,³ and Florian Marquardt^{4,5}

¹*Arnold Sommerfeld Center for Theoretical Physics,
Center for NanoScience and Department of Physics,
Ludwig-Maximilians-Universität München, Theresienstrasse 37, 80333, München, Germany*

²*Department of Physics, McGill University, Montreal, Quebec, Canada H3A 2T8*

³*Institute for Theoretical Physics, Institute for Gravitational Physics,
Leibniz University Hanover, Callinstrasse 38, D-30167 Hanover, Germany*

⁴*Institute for Theoretical Physics, Department of Physics,
Friedrich-Alexander Universität Erlangen-Nürnberg, Staudtstr. 7, 91058 Erlangen, Germany*

⁵*Max Planck Institute for the Science of Light, Günther-Scharowsky-Straße 1/Bau 24, 91058 Erlangen, Germany*

(Dated: October 31, 2018)

In the past few years, coupling strengths between light and mechanical motion in optomechanical setups have improved by orders of magnitude. Here we show that, in the standard setup under continuous laser illumination, the steady state of the mechanical oscillator can develop a non-classical, strongly negative Wigner density if the optomechanical coupling is comparable to or larger than the optical decay rate and the mechanical frequency. Because of its robustness, such a Wigner density can be mapped using optical homodyne tomography. This feature is observed near the onset of the instability towards self-induced oscillations. We show that there are also distinct signatures in the photon-photon correlation function $g^{(2)}(t)$ in that regime, including oscillations decaying on a time scale not only much longer than the optical cavity decay time, but even longer than the mechanical decay time.

By coupling optical and mechanical degrees of freedom, the emerging field of optomechanics provides exciting new opportunities to study the quantum mechanical behavior of macroscopic objects (for reviews see [1, 2]). Recent optomechanical cooling experiments are successfully bringing nanomechanical oscillators into their quantum mechanical ground state [3, 4]. The same optomechanical coupling also promises the possibility of single-quadrature measurements of the resulting mechanical quantum states with the help of the light field [5–7]. For a reproducible and persistent quantum state, such measurements would result in an experimental determination of its full Wigner density via tomography, similar to what has been achieved in microscopic systems, for single ions or photons [8, 9]. The recent advances in fabricating optomechanical devices have drastically improved coupling parameters, *e.g.* for optomechanical crystals [10], in microwave setups [3], and other devices like GaAs disks [11] or toroidal optical microcavity [12]. It will likely be possible relatively soon to achieve optomechanical coupling strengths g_0 at the single-photon level that are comparable to the optical cavity decay rate κ , a feat that has already been achieved in cold atom optomechanical systems [13, 14]. This regime of strongly nonlinear quantum optomechanics promises to pave the way towards generating and detecting novel quantum states in optomechanical systems. It is currently only beginning to be explored theoretically [15–17], although very early work already discussed quantum optomechanical effects in the (unrealistic) absence of any dissipation [18, 19].

In the classical regime, nonlinear dynamics is known to occur when the system is driven by a blue detuned laser. When the input laser power crosses a certain threshold,

the mechanical oscillator will undergo a Hopf bifurcation and start self-induced mechanical oscillations, a phenomenon termed “parametric instability” [20–25]. The quantum dynamics of this regime has first been studied in [15], and there is interesting synchronization behaviour for arrays of coupled oscillators of this type [26].

In this paper, we show that, for strong optomechanical couplings g_0 comparable to or greater than the optical decay rate κ and mechanical frequency ω_M ($g_0/\kappa \gtrsim 1$, $g_0^2/(\kappa \cdot \omega_M) \gtrsim 1$), a large laser driving and an effectively zero temperature thermal bath, a non-classical state of the mechanical oscillator with strongly negative Wigner density can be produced around the onset of self-induced oscillations. Because the state is time-independent, one may use single-quadrature homodyne tomography to experimentally reconstruct its non-classical Wigner density.

In addition, we propose to use the two-point photon correlation function $g^{(2)}(t)$ as an experimentally convenient probe for the peculiar quantum dynamics near the bifurcation. We identify two distinct signatures that enable experimentalists to reliably detect the onset and growth of the self-induced oscillation. We provide an explanation of the non-classical decay of $g^{(2)}(t)$ in both the red and blue-detuned regime.

Within the rotating wave approximation, an optomechanical system can be described by the following standard Hamiltonian:

$$\hat{H} = \hbar(-\Delta + g_0(\hat{b}^\dagger + \hat{b}))\hat{a}^\dagger\hat{a} + \hbar\omega_M\hat{b}^\dagger\hat{b} + \hbar\alpha_L(\hat{a}^\dagger + \hat{a}) + \hat{H}_{\text{diss}}. \quad (1)$$

Here \hat{a}/\hat{b} are the operators for the photon/phonon modes, ω_M is the mechanical frequency and α_L is the laser driving amplitude. $\Delta = \omega_L - \omega_C$ is the detuning of the

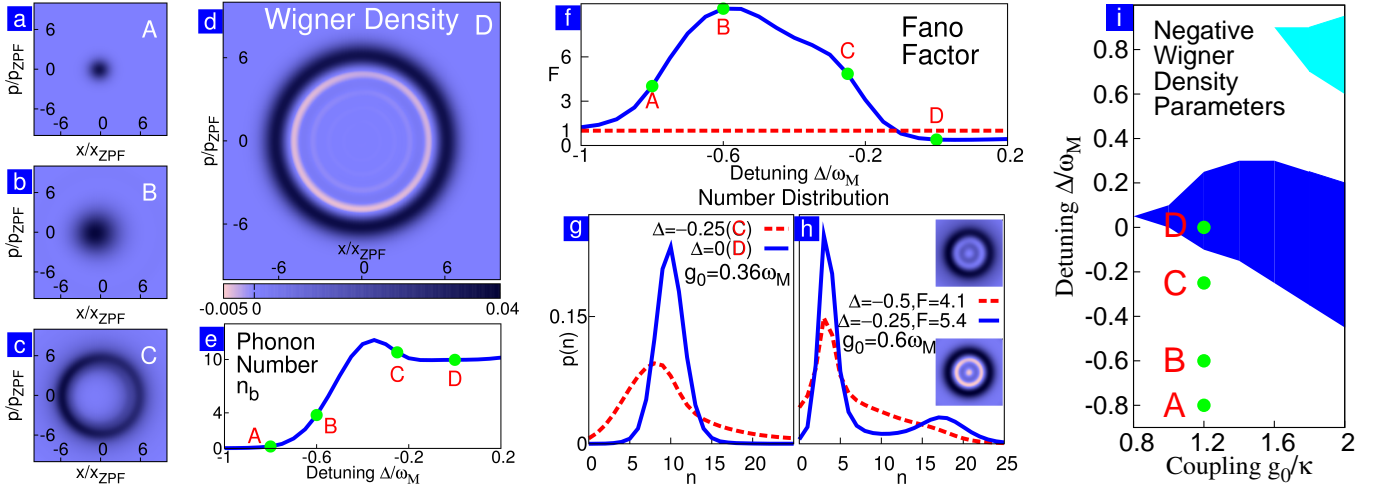


FIG. 1: Non-classical states in an optomechanical system. The laser input α_L is held constant and the laser detuning Δ increases from the steady state “A” to “D”. The mechanical Wigner densities of these states are shown in (a)-(d). x_{ZPF} and p_{ZPF} are zero-point fluctuations of the oscillator’s position and momentum, respectively. Plot (e) shows the start of the self-induced oscillation, where the phonon number n_b of the oscillator rises quickly between state “B” and “C”. As the detuning further increases to “D”, a non-classical mechanical quantum state with *negative* mechanical Wigner density state appears, as shown in (d). In (f) the evolution of the mechanical Fano factor F as a function of Δ is shown. It dips below the Poisson value 1 (dashed line) in non-classical state shown here. In plot (g) and (h), we show that the negative Wigner density states have more sharply peaked phonon number distributions $p(n)$ compared with non-negative states. In (g) the $p(n)$ of state “C” and “D” (plot (c),(d)) are compared. In (h), where $g_0 = 0.6\omega_M$, the negative state (solid line) has two clear peaks in $p(n)$, in contrast to a single smooth peak for the non-negative state (dashed line). The Wigner density of these two states are shown as insets. Finally, in (i) we show two regions in the parameter space of detuning Δ and coupling g_0 where significant negative Wigner density states exist. States “A”-“D” are indicated here. In all plots other physical parameters are $g_0 = 0.36\omega_M, \kappa_M = 0.3\omega_M, \Gamma_M = 0.00147\omega_M, \alpha_L = 0.311\omega_M$, except for (h), where $g_0 = 0.6\omega_M, \alpha_L = 0.186\omega_M$. The intra-cavity photon number is $n_a \approx 0.1-0.7$ when $g_0 = 0.36\omega_M, -\omega_M \leq \Delta \leq 0$.

laser from the cavity’s *unperturbed* resonance (*i.e.* evaluated for *zero mechanical displacement*). g_0 describes the strength of the optomechanical coupling at the single-photon level.

When the dissipative terms in H_{diss} are taken into account, the density matrix $\hat{\rho}$ of the combined photon-phonon system evolves according to the quantum master equation:

$$\frac{d\hat{\rho}}{dt} = \mathcal{L}[\hat{\rho}] = \frac{[\hat{H}, \hat{\rho}]}{i\hbar} + \Gamma\mathcal{D}[\hat{b}, \hat{\rho}] + \kappa\mathcal{D}[\hat{a}, \hat{\rho}]. \quad (2)$$

Here \mathcal{L} is the quantum Liouville operator describing the time evolution of the density matrix $\hat{\rho}$, where we incorporate dissipation in the photon and phonon subsystems with decay rates κ and Γ , respectively. The standard Lindblad term is given by $\mathcal{D}[\hat{O}, \hat{\rho}] = \hat{O}\hat{\rho}\hat{O}^\dagger - \frac{1}{2}(\hat{O}^\dagger\hat{O}\hat{\rho} + \hat{\rho}\hat{O}^\dagger\hat{O})$. Note that we will assume zero bath temperature in our simulations, which will be reachable to a good approximation when GHz-frequency setups (*e.g.* optomechanical crystals) are deployed in dilution refrigerator settings. In this paper, we are interested in the steady state solution of Eq. 2, where all the transient dynamics has died out. This is obtained numerically by finding the density matrix satisfying $\mathcal{L}[\hat{\rho}] = 0$ using

the standard Arnoldi algorithm, as implemented in the ARPACK package. Due to its persistence, this state is ideal for making homodyne measurements of its mechanical Wigner density, in contrast to transient scenarios.

Specifically we are interested in the mechanical Wigner density $W_M(x, p) = \frac{1}{\pi\hbar} \int_{-\infty}^{\infty} \langle x - y | \hat{\rho}_M | x + y \rangle e^{2ipy/\hbar} dy$, where $\hat{\rho}_M$ is the mechanical density matrix, obtained by tracing out the optical degrees of freedom from $\hat{\rho}$. The Wigner density is the quantum analog of the classical Liouville phase space probability density. A negative Wigner density is a strong signature of a non-classical state. Early investigations [15] of the optomechanical instability in the regime around $g_0 \sim \kappa$ did not turned up nonclassical states.

In Fig 1, (a)-(e), we show the overall properties of the steady state solutions. As we increase the laser detuning while keeping the input laser power fixed (points A \rightarrow B \rightarrow C), the phonon number in the mechanical oscillator rises sharply (plot (e)), signaling the onset of the self-induced oscillations. This is also reflected in the mechanical Wigner density $W_M(x, p)$. Below the onset (point “A”), $W_M(x, p)$ is a simple Gaussian, which starts to broaden just below the threshold, as the susceptibility of the system diverges and quantum fluctuations

are strongly amplified (point “B”). Above the threshold, we have a coherent state undergoing circular motion in phase space, but with an undetermined phase, which is the Wigner density observed at point “C” [15, 17].

However, such a simple picture is inadequate for an optomechanical system with $g_0 \sim \kappa$, *i.e.* when one approaches the optomechanical instability deep in the quantum regime [40]. In such a system, we observe that for a range of detuning Δ and laser driving α_L , the mechanical self-induced oscillation produces strongly non-classical states with large negative areas in the Wigner density. This can be seen in the example of Fig. 1 (d). Negative rims, shown in brighter color, develop at amplitudes slightly smaller than the average amplitude of oscillation. Plots (f)-(h) in Fig. 1 analyze negative states more deeply. In state “D”, (f) shows the mechanical Fano factor $F = \frac{\langle \Delta n_b^2 \rangle}{\langle n_b \rangle}$ dips below the coherent state value 1, and its phonon number distribution (g) has a reduced variance. At larger coupling $g = 0.6\omega_M$ (h), the negative state exhibits a sharp peak and a smoother one, as opposed to a single broader peak of the non-negative state [41]. Overall, (f)-(h) show that the negative states are closer to a *single* Fock state *or* a superposition of *few* Fock states as compared with a coherent state [29]. Note, however, the origin of this non-classical state is *not* the same as that in the well-studied micromaser [30–33]. In the micromaser, the mechanism relies crucially on the swapping of a single excitation between an excited atom and cavity over a fixed interaction time. These features are absent in our system.

Fig. 1 (i) maps out the regions in parameter space where negative Wigner densities occur. This ‘phase diagram’ is shown as a function of the “quantum parameter” $\zeta = \frac{g_0}{\kappa}$ [15] and of the laser detuning $\Delta\omega_M$, at a fixed value of the laser driving strength α_L . It has been obtained by solving for the steady state of the optomechanical system under constant illumination, and the Wigner density is considered as nonclassical if a sufficiently large area turns out to be negative. The threshold criterion is a negative area of at least 3% of the positive area, and the minimum value being at least 5% in absolute value of the maximum. The numerical results shown here indicate that, for the parameters considered here, starting at $\frac{g_0}{\kappa} = 0.8$, the negative Wigner density states appear around detuning $\Delta/\omega_M = 0$, and a second negative Wigner density region opens up at $\frac{g_0}{\kappa} = 1.6$, around $\Delta/\omega_M = 0.9$ at the first blue sideband, where the instability is driven efficiently. The phonon number distribution displays a pronounced narrowing, getting closer to a single or few mechanical Fock states. However, we find that still many photon/phonon levels are involved in the dynamics in the regime considered here, and there seems to be no simple explanation involving only a few levels.

These *steady-state* non-classical Wigner densities could be reconstructed via optomechanical Quantum Non-

demolition quadrature detection [5, 6] and subsequent quantum state tomography [34]. This merely involves illumination with another amplitude-modulated laser beam for read-out, as explained in [6]. When observed, these would provide an accessible example of non-classical states in a fabricated mesoscopic mechanical object. To date, there has been no experimental observation of non-classical Wigner densities in the domain of micro- or nanomechanical structures. The experiment that came closest to that goal, and in the process did produce non-classical mechanical Fock states, employed a complex multi-layered superconducting circuit with piezoelectric coupling to a superconducting qubit and ultrafast pulse sequences [35]. Furthermore in their setup the resonator lifetime is too short to permit the reconstruction of the full Wigner density. By contrast, once optomechanical parameters can be improved to reach the single-photon strong coupling regime, the scheme discussed here would be relatively straightforward, being based on continuous laser illumination of an optomechanical setup whose fabrication is much less complex as it involves only one material. Recently a coupling $g_0/\kappa \approx 0.007$ has been achieved in an optomechanical crystal system [36] and further improvement is expected in that setup. In addition, there is the possibility that the parameters required here may be reached in cold atom optomechanical setups [13, 14].

The full mechanical state reconstruction in the nonlinear quantum regime is an enticing and challenging goal. Nevertheless, it requires many experimental runs. It will be helpful to have other means of optically probing the quantum dynamics of the system around the onset of the instability. A very suitable probe for the dynamics is provided by the two-point photon correlation function:

$$g^{(2)}(t) = \frac{\langle \hat{a}_\tau^\dagger \hat{a}_{\tau+t}^\dagger \hat{a}_{\tau+t} \hat{a}_\tau \rangle}{(\langle \hat{a}_\tau^\dagger \hat{a}_\tau \rangle)^2}. \quad (3)$$

$\langle \dots \rangle$ denotes the average over $\hat{\rho}$. Here we employ the two-point correlator for the intra-cavity photon field, extractable from our numerical simulations. However, we emphasize that it can be shown using input-output theory (See Appendix A-1) that Eq. 3 also directly provides the $g^{(2)}$ function for the fluctuations of the output optical field.

In steady state, $g^{(2)}$ does not depend on the initial time τ . Photon correlations are readily accessible in quantum optics experiments today with single-photon detectors (*e.g.* using a Hanbury-Brown Twiss setup), and they have been successfully employed to characterize the change of photonic statistics upon transmission through nonlinear systems. The most important example is photon anti-bunching in the resonance fluorescence of single photon emitters, which has recently also been predicted to occur in optomechanical systems for sufficiently strong coupling [16].

As can be seen in Fig. 2, there are clear signatures in

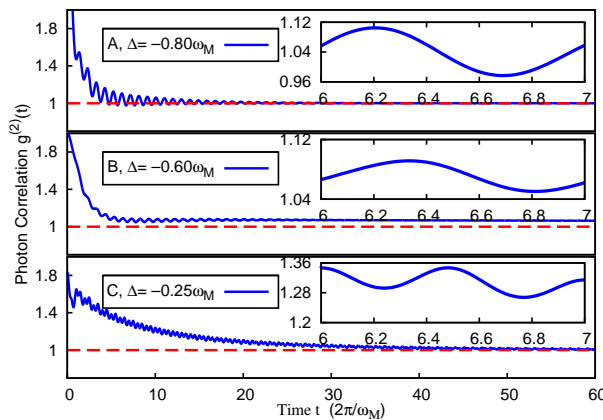


FIG. 2: Time-dependence of photon-photon correlations near the regime of quantum optomechanical oscillations. “A,B,C” labels the same states as in Fig. 1. These plots show that there is a remarkably slow long-term decay near the onset of self-induced oscillations at point “B” (see main text). Inset also shows the appearance of higher harmonics at point “C”.

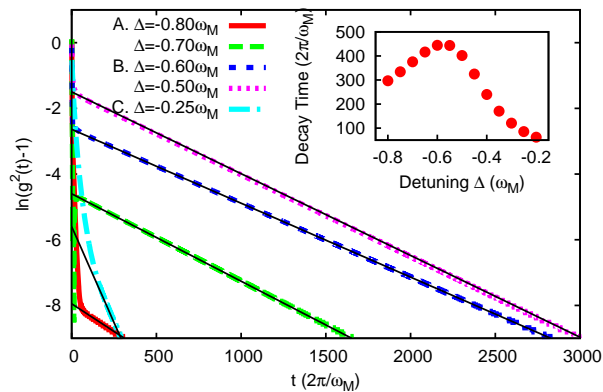


FIG. 3: Quantifying the slow approach of $g^{(2)}(t) \rightarrow 1$ near the onset of the self-induced oscillations, as observed in Fig. 2. $g^{(2)}(t) - 1$ obeys an exponential decay e^{-t/τ_g} in the long-time limit $t \rightarrow \infty$. The inset shows the decay time τ_g peaking toward very large values around point B, *i.e.* $\Delta = 0.6\omega_M$.

the photon correlator around the onset of parametric instability (point B). In particular, $g^{(2)}(t)$ persists at some value above unity over a very long time (middle panel, Fig. 2). It can be proven (see Appendix A-2) that as long as the steady state of the system is not degenerate, we always have $g^{(2)}(t) \rightarrow 1 + \alpha \exp(-t/\tau_g)$ in the long-time limit $t \rightarrow \infty$. Here the decay rate is $1/\tau_g = \text{Re}(\lambda_1)$, where λ_1 is the eigenvalue of the Liouville operator \mathcal{L} in Eq. 2 with the largest non-zero real part, characterizing the slowest decay in the system. This can be verified by plotting $\ln(g^{(2)}(t) - 1)$ to extract τ_g , which indeed agrees with the λ_1 obtained from \mathcal{L} (see Fig. 3). As can be seen in the inset, τ_g rises strongly around the start of the self-induced oscillation (point B). This is connected to the fact that the overall mechanical damping rate goes

to zero near the Hopf bifurcation [23].

The second signature in $g^{(2)}$ is the appearance of higher harmonics when the self-induced oscillations are fully developed (see insets of Fig. 2). To understand these in a semiclassical picture, we approximate the photon correlator via the classical intensity correlator, $\langle |\alpha(t+\tau)|^2 |\alpha(\tau)|^2 \rangle_\tau$. The light amplitude $\alpha(t) = e^{i\phi(t)} \sum_n \alpha_n e^{in\omega_M t}$ is modulated harmonically by the mechanical oscillations, as detailed in [23]. In Appendix A-3 we show that a fully developed mechanical self-induced oscillation results in higher harmonics in $g^{(2)}$. To understand the *decay* of the resulting oscillations in the $g^{(2)}$, we take into account the mechanical phase diffusion induced by the radiation pressure shot noise. [37] presented the first analysis of the quantum contribution to phase diffusion in the parametric instability regime. Here we follow a slightly modified approach. The phase fluctuates according to $\delta\phi(t) = (m\omega_M A)^{-1} \int_0^t dt' \delta F(t') \cos(\omega_M t')$, which yields:

$$\text{Var}(\delta\phi(t)) = \frac{1}{(m\omega_M A)^2} \frac{t}{4} (S_{FF}(\omega_M) + S_{FF}(-\omega_M)),$$

where S_{FF} is the force noise spectrum (see [38]). Thus:

$$\langle |\alpha(t+\tau)|^2 |\alpha(\tau)|^2 \rangle_\tau = \sum_{n=-\infty}^{+\infty} Z_n e^{in\omega_M t} e^{-n^2 \langle \delta\phi(t)^2 \rangle / 2},$$

where $Z_n = |\sum_{m=-\infty}^{\infty} \alpha_m \alpha_{m-n}^*|^2$. This theory explains qualitatively the shape of the correlator even deep in the quantum regime (Appendix A-4). Finally, we note that in the red detuned regime, the photon correlator decay can be described by the optomechanical cooling rate (see Appendix A-4).

To summarize, in this paper we investigated quantum signatures of light and mechanics for an optomechanical system in the parametric instability regime. We found that, at strong optomechanical coupling ($g_0 \sim \kappa, g_0^2 \sim (\kappa \cdot \omega_M)$), for a range of detuning and input power, the steady state mechanical Wigner density contains strong negative parts, signaling stable non-classical states. Single-quadrature homodyne measurements can be used to reconstruct the Wigner density. In addition, the two-point photon correlator $g^{(2)}(t)$ displays two clear signatures near the onset of parametric instability. Finally we explained the slow long-time decay of the photon correlations as due to the mechanical phase diffusion induced by photon shot noise. One should note that experimental observation of some of these photon correlation features does not require being in the nonlinear quantum regime and could succeed even in existing setups.

F.M. acknowledges the DFG (Emmy-Noether) and an ERC Starting Grant. F.M. and A.C. acknowledge the DARPA ORCHID program. J.Q. acknowledges the sup-

port of DFG SFB 631 and NIM. K.H acknowledges the support through QUEST.

Appendices

A-1. Correlation Function: from Intra-cavity to Output Field

Here we summarize how the calculation of the $g^{(2)}$ -function for the output field \hat{a}_{out} can be traced back to calculating $g^{(2)}$ for the intra-cavity field \hat{a} , following [39]. We are interested in the normally ordered two-time correlation function of the output field

$$g^{(2)}(t) = \frac{\langle \hat{a}_{\text{out}}^\dagger(\tau) \hat{a}_{\text{out}}^\dagger(t+\tau) \hat{a}_{\text{out}}(t+\tau) \hat{a}_{\text{out}}(\tau) \rangle}{\langle \hat{a}_{\text{out}}^\dagger(\tau) \hat{a}_{\text{out}}(\tau) \rangle^2}. \quad (\text{A-1})$$

We substitute the input-output relation $\hat{a}_{\text{out}}(t) = \hat{a}_{\text{in}}(t) + \sqrt{\kappa} \hat{a}(t)$, and use that $\hat{a}^\dagger(\tau)$ commutes with $\hat{a}_{\text{in}}^\dagger(t+\tau)$, and $\hat{a}(t+\tau)$ commutes with $\hat{a}_{\text{in}}(\tau)$ for $t \geq 0$ as a consequence of causality, see [39] for details. This permits us to bring the two time correlation function to a form where the $\hat{a}_{\text{in}}^\dagger$ stand to the left, and the \hat{a}_{in} to the right of all other operators. Moreover, note that for vacuum input $\hat{a}_{\text{in}} \rho_{\text{in}} = \rho_{\text{in}} \hat{a}_{\text{in}}^\dagger = 0$. This ultimately establishes the identity

$$\begin{aligned} & \langle \hat{a}_{\text{out}}^\dagger(\tau) \hat{a}_{\text{out}}^\dagger(t+\tau) \hat{a}_{\text{out}}(t+\tau) \hat{a}_{\text{out}}(\tau) \rangle \\ &= \kappa^2 \langle \hat{a}^\dagger(\tau) \hat{a}^\dagger(t+\tau) \hat{a}(t+\tau) \hat{a}(\tau) \rangle, \end{aligned} \quad (\text{A-2})$$

such that the normalized correlation function for the output field is *identical* to the normalized correlation function of the intra-cavity field. This is what we calculated in Eq. (3) of the main text.

A-2. Proof Concerning the Longtime Limit of $g^{(2)}(t)$

In this section we give a proof that the $g^{(2)}(t)$ defined in Eq. 3 of the main text, approaches one as $t \rightarrow \infty$.

We can rewrite the unnormalized correlation function (the numerator of Eq. 3 of the main text) as follows:

$$\begin{aligned} g_0^{(2)}(t) &= \text{tr}[\hat{\rho} \hat{a}_\tau^\dagger \hat{a}_{t+\tau}^\dagger \hat{a}_{t+\tau} \hat{a}_\tau] \\ &= \text{tr}[(\hat{a}_\tau \hat{\rho} \hat{a}_\tau^\dagger) \hat{a}_{t+\tau}^\dagger \hat{a}_{t+\tau}] \\ &= \text{tr}[(\hat{a}_\tau \hat{\rho} \hat{a}_\tau^\dagger) e^{\frac{i\hat{H}t}{\hbar}} \hat{a}_\tau^\dagger \hat{a}_\tau e^{-\frac{i\hat{H}t}{\hbar}}] \\ &= \text{tr}[\hat{a}_\tau^\dagger \hat{a}_\tau e^{-\frac{i\hat{H}t}{\hbar}} (\hat{a}_\tau \hat{\rho} \hat{a}_\tau^\dagger) e^{\frac{i\hat{H}t}{\hbar}}] \\ &= \text{tr}[\hat{a}_\tau^\dagger \hat{a}_\tau e^{\mathcal{L}t} \hat{\rho}']. \end{aligned} \quad (\text{A-3})$$

Here $\hat{\rho}' = \hat{a}_\tau \hat{\rho} \hat{a}_\tau^\dagger$ and $e^{\mathcal{L}t} \hat{\rho}'$ is its time evolution under the quantum Liouville operator Eq. 2 of the main text. In the last step we use the quantum regression approximation.

Let us now consider the right eigenvectors of \mathcal{L} :

$$\mathcal{L} \hat{\rho}_n = \lambda_n \hat{\rho}_n. \quad (\text{A-4})$$

Here we rank $\hat{\rho}_n$ in descending order of $\text{Re } \lambda_n$. Assuming the steady state $\lambda_0 = 0$ is not degenerate, we have $\text{Re } \lambda_n < 0$ for $n > 1$. Since the trace is conserved in the time evolution according to Eq. 2 of the main text, $\text{tr}(\hat{\rho}_n) = 0$ for $n > 0$ and $\text{tr}(\hat{\rho}_0) = 1$ (by normalization).

Expand the $\hat{\rho}' = \hat{a}_\tau \hat{\rho} \hat{a}_\tau^\dagger$ in eigenvectors $\hat{\rho}_n$:

$$\hat{\rho}' = \sum_n c_n \hat{\rho}_n, \quad (\text{A-5})$$

$$e^{\mathcal{L}t} \hat{\rho}' = \sum_n c_n \hat{\rho}_n e^{\lambda_n t}. \quad (\text{A-6})$$

we can then evaluate the correlator in Eq. A-3 as $t \rightarrow \infty$:

$$\begin{aligned} g_0^{(2)}(t \rightarrow \infty) &= \lim_{t \rightarrow \infty} \text{tr}[\hat{a}_\tau^\dagger \hat{a}_\tau e^{\mathcal{L}t} \hat{\rho}'] \\ &= \text{tr}[\hat{a}_\tau^\dagger \hat{a}_\tau c_0 \hat{\rho}_0] \\ &= c_0 \text{tr}[\hat{a}_\tau^\dagger \hat{a}_\tau \hat{\rho}_0] \\ &= c_0 \text{tr}[\hat{a}_\tau^\dagger \hat{a}_\tau \hat{\rho}]. \end{aligned} \quad (\text{A-7})$$

In the last step we use the fact that at time τ the system is in a steady state where the photon number no longer changes with time. Taking the trace of both sides of Eq. A-5 and utilizing the properties of $\text{tr}(\hat{\rho}_n)$ discussed above, we have:

$$c_0 = \text{tr}[\rho'] = \text{tr}[\hat{a}_\tau \hat{\rho} \hat{a}_\tau^\dagger] = \text{tr}[\hat{a}_\tau^\dagger \hat{a}_\tau \hat{\rho}] = \langle \hat{a}_\tau^\dagger \hat{a}_\tau \rangle. \quad (\text{A-8})$$

Thus we arrive at:

$$\begin{aligned} g^{(2)}(t \rightarrow \infty) &= \frac{g_0^{(2)}(t \rightarrow \infty)}{(\langle \hat{a}_\tau^\dagger \hat{a}_\tau \rangle)^2} \\ &= \frac{(\text{tr}[\hat{a}_\tau^\dagger \hat{a}_\tau \hat{\rho}])^2}{(\langle \hat{a}_\tau^\dagger \hat{a}_\tau \rangle)^2} \\ &= 1. \end{aligned} \quad (\text{A-9})$$

Finally, we point out that the leading term governing the asymptotic approach of $g^{(2)} \rightarrow 1$ is λ_1 in Eq. A-4, since it has the slowest exponential decay in Eq. A-6. This gives the asymptotic behavior of $g^{(2)}(t)$ shown in the main text.

A-3. Correlation Function: Semiclassical Picture

Under typical experimental conditions, when the classical self-induced oscillation starts, the mechanical motion is to a good approximation harmonic $x(t) \approx \bar{x} + A \cos(\omega_M t)$. The laser amplitude, influenced by the mechanical oscillation, will contain higher harmonics [23] $\alpha(t) = e^{i\phi(t)} \sum_n \alpha_n e^{in\omega_M t}$, where

$$\alpha_n = \frac{\alpha_L J_n(-g_0 A)}{-n\omega_M + (\Delta + g_0 \bar{x}) + i\kappa/2} \quad (\text{A-10})$$

and $\phi(t) = g_0 A \sin(\omega_M t)$. Here we take the length unit to be the mechanical zero point fluctuation x_{ZPF} and frequency unit to be ω_M . $J_n(x)$ is the n -th order Bessel function. The oscillation amplitude A and equilibrium position \bar{x} can be determined self-consistently. We can express $g^{(2)}(t)$ in terms of the coefficients in Eq. A-10:

$$Z_n = \left| \sum_{m=-\infty}^{\infty} \alpha_m \alpha_{m-n}^* \right|^2, \quad \langle |\alpha(\tau)|^2 \rangle_\tau = \sum_{n=-\infty}^{\infty} |\alpha_n|^2 = Z_0.$$

$$\langle |\alpha(t+\tau)|^2 |\alpha(\tau)|^2 \rangle_\tau = Z_0 + 2 \sum_{n=1}^{\infty} \cos(n\omega_M t) Z_n \quad (\text{A-11})$$

In this paper we're interested in the strongly quantum regime where $g_0 \approx \kappa$, thus in the sideband resolved regime we have $g_0/\omega_M < 1$. From Eq. A-10 we see that only when $A \gg x_{\text{ZPF}}$ would there be significant contribution of higher harmonics in the light amplitude $\alpha(t)$, which, as can be seen from Eq. A-11 is also the condition of having higher harmonics in $g^{(2)}(t)$. This explains qualitatively the appearance of higher harmonics in the insets of Fig. 2 in the main text when the quantum self-induced oscillation gains large amplitude.

A-3. Correlation Function: Quantum Fluctuation

However, even when the self-induced oscillation has amplitude much larger than the x_{ZPF} , there are important quantum effects that are not accounted for by Eq. A-10 and Eq. A-11. As seen in Fig. A-1, the classical solution (bottom) is fully periodic, as there is a balance between the optical and mechanical dissipation and laser driving. However, over the period of 60 cycles, the amplitude of the quantum mechanical $g^{(2)}(t)$ decays significantly (top three panels, blue curves). We can account for this decay by calculating the effect of shot noise fluctuations in the radiation pressure force $F(t) = (\hbar\omega_R/L)\hat{a}(t)^\dagger\hat{a}(t)$ on the phase ϕ of the mechanical oscillations:

$$\delta\phi(t) = \frac{1}{m\omega_M A} \int_0^t dt' F(t') \cos(\phi(t')), \quad (\text{A-12})$$

$$\text{Var}(\delta\phi(t)) = \frac{1}{(m\omega_M A)^2} \frac{t}{4} (S_{FF}(\omega_M) + S_{FF}(-\omega_M)).$$

The noise spectrum of the radiation force is can be easily computed [38]:

$$S_{FF}(\omega) = \left(\frac{\hbar\omega_R}{L} \right) \bar{n}_p \frac{\kappa}{(\omega + \Delta)^2 + (\kappa/2)^2}. \quad (\text{A-13})$$

The fluctuations of the mechanical oscillator's phase feed back to the time-dependence of optical amplitude. Thus, under the semi-classical assumption where we take into account the photon shot noise but still treat the photon

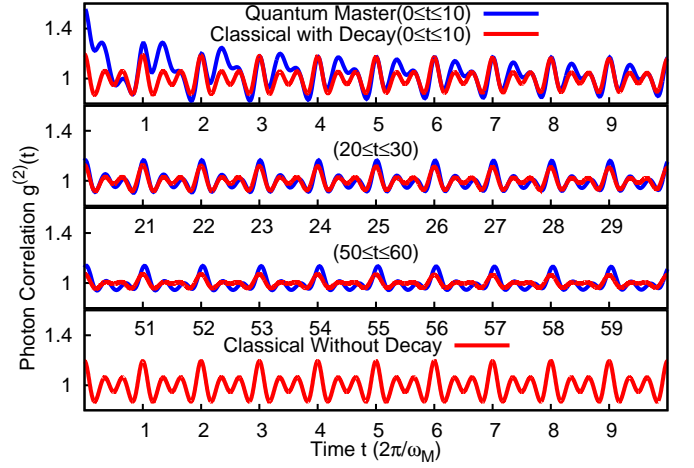


FIG. A-1: Semiclassical approximation for photon correlations in the parametric instability regime of optomechanics. By adding the mechanical phase-diffusion to the classical light field dynamics (red), one can qualitatively account for the slow long-time decay of the photon correlator $g^{(2)}(t)$ in the full quantum simulation (blue). The lowest panel plots the classical solution without phase diffusion (here $\Delta = \omega_M$).

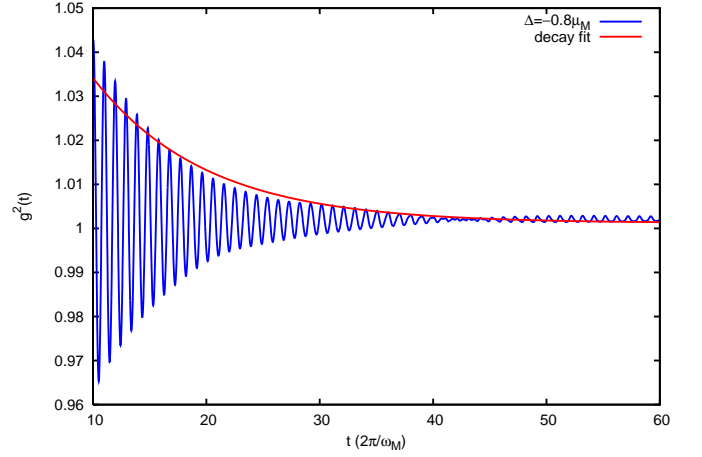


FIG. A-2: The decay of the correlation function $g^{(2)}(t)$ in the red-detuned regime $\Delta = -0.8\omega_M$ can be qualitatively accounted for with Γ_{opt} obtained from optomechanical cooling.

amplitude classically, we can modify Eq. A-11 to be:

$$\langle |\alpha(t+\tau)|^2 |\alpha(\tau)|^2 \rangle_\tau = \sum_{n=-\infty}^{\infty} Z_n e^{in\omega_M t} \langle e^{in(\delta\phi(t+\tau) - \delta\phi(t))} \rangle$$

$$= Z_0 + 2 \sum_{n=1}^{\infty} Z_n \cos(n\omega_M t) e^{-\frac{n^2}{2} \text{Var}(\delta\phi(t))}.$$

Here we assume the phase fluctuation $\delta\phi$ is Gaussian. The result of this semi-classical accounting of the photon shot noise can be seen in the red curves in the top three panels of Fig. A-1. We can see that this simple analysis

can account qualitatively for the decay of the $g^{(2)}(t)$ in the large amplitude self-induced oscillation regime.

Finally, as we see in Fig. A-2, there are also significant oscillation structure and decay for the $g^{(2)}(t)$ in the so-called red detuned regime, before the start of the self-induced oscillation. This regime cannot be understood at all by the classical picture, since classically the system has no dynamics there. The oscillation in $g^{(2)}(t)$ can be understood as the dynamical response of the mechanical oscillator to the quantum fluctuation of the photon field. The decay can then be modeled using the theory of the optomechanical cooling of the mechanical oscillation in the red detuned regime, giving a cooling rate

$$\Gamma_{opt} = \frac{x_{ZPF}^2}{\hbar^2} [S_{FF}(\omega_M) - S_{FF}(-\omega_M)]. \quad (\text{A-14})$$

Here S_{FF} is the same noise spectrum given by Eq. A-13. As seen in Fig. A-2, this rate gives a qualitative account for the decay rate of $g^{(2)}(t)$ in the red-detuned regime.

-
- [1] F. Marquardt and S. M. Girvin, *Physics* **2**, 40 (2009)
- [2] T. J. Kippenberg and K. J. Vahala, *Science* **321**, 1172 (2008)
- [3] J. D. Teufel *et al.*, *Nature* **475**, 359 (2011)
- [4] J. Chan, T. P. M. Alegre, A. H. Safavi-Naeini, J. T. Hill, A. Krause, S. Groblacher, M. Aspelmeyer, and O. Painter, *Nature* **478**, 89 (2011)
- [5] V. B. Braginsky, F. Y. Khalili, and K. S. Thorne, *Quantum Measurement* (Cambridge University Press, 1995)
- [6] A. A. Clerk, F. Marquardt, and K. Jacobs, *New Journal of Physics* **10**, 095010 (2008)
- [7] J. B. Hertzberg, T. Rocheleau, T. Ndukum, M. Savva, A. A. Clerk, and K. C. Schwab, *Nature Physics* **6**, 213 (2010)
- [8] D. Leibfried, D. M. Meekhof, B. E. King, C. Monroe, W. M. Itano, and D. J. Wineland, *Phys. Rev. Lett.* **77**, 4281 (1996)
- [9] A. I. Lvovsky, H. Hansen, T. Aichele, O. Benson, J. Mlynek, and S. Schiller, *Phys. Rev. Lett.* **87**, 050402 (2001)
- [10] M. Eichenfield, J. Chan, R. M. Camacho, K. J. Vahala, and O. Painter, *Nature* **462**, 78 (2009)
- [11] L. Ding *et al.*, *Phys. Rev. Lett.* **105**, 263903 (2010)
- [12] E. Verhagen, S. Deléglise, S. Weis, A. Schliesser, and T. K. Kippenberg, *Nature* **482**, 63 (2012)
- [13] K. W. Murch, K. L. Moore, S. Gupta, and D. M. Stamper-Kurn, *Nature Physics* **4**, 561 (2008)
- [14] F. Brennecke, S. Ritter, T. Donner, and T. Esslinger, *Science* **322**, 235 (2008)
- [15] M. Ludwig, B. Kubala, and F. Marquardt, *New Journal of Physics* **10**, 095013 (2008)
- [16] P. Rabl, *Phys. Rev. Lett.* **107**, 063601 (2011)
- [17] A. Nunnenkamp, K. Børkje, and S. M. Girvin, *Phys. Rev. Lett.* **107**, 063602 (2011)
- [18] S. Mancini, V. I. Man'ko, and P. Tombesi, *Phys. Rev. A* **55**, 3042 (1997)
- [19] S. Bose, K. Jacobs, and P. L. Knight, *Phys. Rev. A* **56**, 4175 (1997)
- [20] V. Braginsky and A. Manukin, *Soviet Physics JETP* **25**, 653 (1967)
- [21] T. J. Kippenberg, H. Rokhsari, T. Carmon, A. Scherer, and K. J. Vahala, *Phys. Rev. Lett.* **95**, 033901 (2005)
- [22] T. Carmon, H. Rokhsari, L. Yang, T. Kippenberg, and K. Vahala, *Phys. Rev. Lett.* **94**, 223902 (2005)
- [23] F. Marquardt, J. G. E. Harris, and S. M. Girvin, *Phys. Rev. Lett.* **96**, 103901 (2006)
- [24] C. Metzger, M. Ludwig, C. Neuenhahn, A. Ortlieb, I. Favero, K. Karrai, and F. Marquardt, *Physical review Letters* **101**, 133903 (2008)
- [25] I. S. Grudin, H. Lee, O. Painter, and K. J. Vahala, *Physical Review Letters* **104**, 083901 (2010)
- [26] G. Heinrich, M. Ludwig, J. Qian, B. Kubala, and F. Marquardt, *Phys. Rev. Lett.* **107**, 043603 (2011)
- [27] Another necessary condition is that $g_0^2/(\kappa \cdot \omega_M)$ is not much smaller than one
- [28] Note here, due to the two-peak structure, the Fano factor of the negative Wigner density state remains above one
- [29] D. A. Rodrigues and A. D. Armour, *Phys. Rev. Lett.* **104**, 053601 (2010)
- [30] P. Filipowicz, J. Javanainen, and P. Meystre, *J. Opt. Soc. Am. B* **3**, 906 (Jun 1986)
- [31] P. Meystre, G. Rempe, and H. Walther, *Opt. Lett.* **13**, 1078 (Dec 1988)
- [32] J. Krause, M. O. Scully, and H. Walther, *Phys. Rev. A* **36**, 4547 (Nov 1987)
- [33] B. T. H. Varcoe, S. Brattke, and H. Walther, *Journal of Optics B: Quantum and Semiclassical Optics* **2**, 154 (2000)
- [34] A. I. Lvovsky and M. G. Raymer, *Reviews of Modern Physics* **81**, 299 (2009)
- [35] A. D. O'Connell, M. Hofheinz, M. Ansmann, R. C. Bialczak, M. Lenander, E. Lucero, M. Neeley, D. Sank, H. Wang, M. Weides, J. Wenner, J. M. Martinis, and A. N. Cleland, *Nature* **464**, 697 (2010)
- [36] J. Chan, A. H. Safavi-Naeini, J. T. Hill, S. Meenehan, and O. Painter, *Applied Physics Letters* **101**, 081115 (2012)
- [37] K. J. Vahala, *Phys. Rev. A* **78**, 023832 (2008)
- [38] F. Marquardt, J. P. Chen, A. A. Clerk, and S. M. Girvin, *Phys. Rev. Lett.* **99**, 093902 (2007)
- [39] C. W. Gardiner and P. Zoller, *Quantum Noise*, 3rd ed. (Springer, 2010)
- [40] Another necessary condition is that $g_0^2/(\kappa \cdot \omega_M)$ is not much smaller than one
- [41] Note here, due to the two-peak structure, the Fano factor of the negative Wigner density state remains above one